Accepted manuscript doi:
10.1680/jphmg.20.00030

Accepted manuscript doi:
10.1680/jphmg.20.00030

Submitted: 16 July 2019

Published online in 'accepted manuscript' format: 27 October 2020

Manuscript title: Centrifuge study of *p-y* curves for vertical-horizontal static loading of piles in sand

Authors: Wenjun Lu[1], Amir M. Kaynia[2] and Ga Zhang[3]

Affiliations: [1]Department of Civil and Environmental Engineering, Hong Kong University of Science and Technology, Hong Kong, China; [2]Norwegian Geotechnical Institute, Oslo, Norway and [3]State Key Laboratory of Hydroscience and Engineering, Tsinghua University, Beijing, P R China

Corresponding author: Ga Zhang, State Key Laboratory of Hydroscience and Engineering, Tsinghua University, Beijing, 100084, P R China. Tel./Fax: 86-10-62795679.

E-mail: zhangga@tsinghua.edu.cn

Accepted manuscript doi:
10.1680/jphmg.20.00030

Abstract

Pile foundations for offshore structures are subjected to vertical-horizontal load combinations. The current design method separately analyzes horizontal and vertical responses of piles without considerations of the combined effect of the loads on soil-pile interaction. However, there is experimental and numerical evidence that lateral behavior of a pile-soil system can be affected by both axial compression and tension load on the pile. In this study, two single-pile and two tripod-pile centrifuge model tests under different loading conditions were analyzed to investigate the influence of combined loads on the lateral response of soil-pile system. The displacement and the bending moment were measured and analyzed to highlight the behavior of pile-soil system under different loading conditions. The *p-y* curves for the different tests were calculated and compared to reveal the influence of axial load component on the lateral behavior of soil-pile systems. It is concluded that compared with pure lateral loading, the *p-y* curves of piles under compression are steeper because of soil densification effect, while the opposite is observed under tension load that is the *p-y* curves are gentler.

Keywords: Centrifuge model test; Load combination; *p-y* curve; Soil-structure interaction; Pile

Accepted manuscript doi:
10.1680/jphmg.20.00030

1 INTODUCTION

Pile foundations for offshore structures are subjected to vertical-horizontal load combinations. For instance, piles of oil platforms are under considerable vertical gravity loads combined with lateral thrusts due to wind and wave actions, and piles in tripod or jacket foundation for offshore wind turbines are subjected to simultaneous axial compression (or tension) and horizontal bending (Zhu et al. 2014; Lu et al. 2016). The current design method deals with the horizontal and vertical response of piles separately, that is without consideration of the soil response due to combined loads. However, evidence indicate that lateral behavior of pile-soil systems can be affected by both axial compression and tension.

By means of full-size in-situ test (Sorochan and Bykov 1976; Karasev et al. 1977) and 1g model test (Zhao et al. 2015), it has been observed that axial compression load could increase the lateral resistance of piles in sand. Such a conclusion has also been confirmed by several numerical and theoretical analyses (Karthigeyan et al. 2006; Chatterjee and Choudhury 2015). However, a number of other works have reached an opposite conclusion that axial compression decreases the horizontal bearing capacity in some situations by model tests (Zhukov 1978; Lee et al. 2011) and numerical analyses (Reddy and Ramasamy 1973; Madhav and Sarma 1982). The influence of uplift load on lateral pile behavior were also studied by numerical simulations (Mroueh and Shahrour 2007; Achmus et al. 2009), field tests (Ismael, 1989) and model tests (Darr et al. 1990; Reddy and Ayothiraman 2015). However, these researches mainly focused on behavioral observations. Therefore, analyses are still required to clarify the mechanism of the influence of vertical loads on the horizontal response of a pile.

Accepted manuscript doi:
10.1680/jphmg.20.00030

The most common approach for analysis of lateral response of piles is by *p*-*y* curves, which simplifies the lateral soil-pile interaction by a series of independent nonlinear springs relating the resistance *p* to the corresponding horizontal displacement *y*. Matlock (1970) and Reese et al. (1974) respectively set up *p*-*y* curves for soft clay and sand based on field tests. Later, other researchers modified the *p*-*y* curves for various pile-soil conditions (Stevens and Audibert 1979; Zhang and Chen 1992; Romo and Ovando-Shelley 1998; Dewaikar and Patil 2006; Klinkvort and Hededal 2014; Byrne et al. 2017; Jeanjean et al. 2017). However, all these researches are on the basis of pure lateral loading tests. In order to modify *p*-*y* curve method for combined loading conditions, pile foundation tests under different vertical-horizontal load combinations are urgently needed.

Centrifuge model testing is an economical and effective way to simulate geotechnical problems, which has been widely used to investigate soil-pile interactions. Lu and Zhang (2018) conducted a series of single-pile tests with different vertical-horizontal load combinations, from which the *P*-Δ effect and soil densification effect of vertical load were revealed. *P*-Δ effect refers to the observation that the axial force introduces an additional bending moment after the lateral deformation of the pile. Soil densification effect refers to that the vertical compression increases the confining stress and the stiffness of soil neighbouring the pile. In this study, two single pile tests and two tripod-pile tests under different loading conditions were analyzed to investigate how of *p*-*y* curves are influenced by different load combinations. The objectives of this paper include: (1) to describe single pile and tripod-pile centrifuge model tests under different loading conditions; (2) to observe the lateral responses of pile-soil systems under different load combinations; (3) to develop a reliable process to calculate p-y curves of piles based on centrifuge test data; (4) to demonstrate the influence of vertical loads on *p*-*y* curves under different load combinations.

2 TEST CONFIGURATIONS

2.1 Devices

The tests in this study were conducted in the 50 g-ton geotechnical centrifuge with a radius of 2.25 m at Tsinghua University. The model container was installed with a transparent wall on a lateral side for observation and measurement of displacements. An automated hydraulic loading system that fixed on the top of the container was employed to apply horizontal load

Accepted manuscript doi:
10.1680/jphmg.20.00030

in-flight. This loading system consisted of a hydraulic cylinder, a lubricant pump, and a control module, with a maximum loading capacity of 10 kN (Lu et al. 2016).

2.2 Model

Silica sand with effective and mean particle sizes D_{10} = 0.107 mm and D_{50} = 0.192mm respectively was used to represent offshore soil conditions. The grain-size distribution curve of this sand is shown in Fig. 1 with parameters summarized in Table 1. The dry sand was compacted layer by layer to a design height of 470 mm with a relative density of 0.58. The friction angle, φ', was 32 degrees according to the direct shear tests. Afterwards, the model container was placed into a sealed box for vacuum saturation (Fig. 2). A vacuum pump was used to exhaust the inside air through the top air outlet. Meanwhile, water slowly flowed into the model container from the bottom water inlet, using a drip nozzle and a water valve. The vacuum saturation process lasted for around 2 days until the water level in the sand was 50 mm above the ground level.

Because of the symmetries of the pile and loads, half-models were used to observe the displacements of soil-pile system in the symmetric plane through the transparent wall. Silicone oil was smeared between the glass and the soil-pile model in order to diminish the friction in the symmetric plane. The piles were jacked into the sand under 1 g after the whole sand base was prepared and saturated. All the pile models were made of aluminum with a diameter of 20 mm and a length of 330 mm, representing a prototype with 1 m diameter and 16.5 m length at the 50 g level. With a Young's modulus of 70 GPa, the flexural stiffness of the pile equals to 3.43 GNm^2 at prototype, which is equivalent to a steel pipe pile with a diameter of 1 m and a wall thickness of 5 cm by assuming the Young's modulus of steel as 200 GPa,

Three different types of models, half single-pile, half tripod-pile and whole single-pile foundations were used in this study for different load combinations. Fig. 3 provides the sketch and photo of the single pile model. A half pile (Pile S) was placed against the transparent wall with a cylindrical loading cap installed on the top to ensure the loading center to be within the symmetrical plane. The distance between the horizontal load application point and ground level was 145 mm. Steel pieces were fixed onto the pile cap to provide a constant vertical load in tests at a high g level. The pile was free-head with both rotation and displacement freedom. More details of single pile tests have been described by Lu and Zhang (2018). Fig. 4 shows the sketch and photo of the tripod-pile model. A half pile (Pile A) and a full pile (Pile B) were placed at the vertexes of an equilateral triangle with an edge length of 200 mm. The superstructure of the tripod-pile model was a steel triangle trusses with the total weight of 0.68 kg, which consisted of a vertical tube with a diameter of 40 mm and four inclined tubes with a diameter of 20 mm. The thickness of the pipe wall of the triangle trusses was 1 mm. Triangle trusses were strongly fixed to the pile caps above the ground for applying the loads, so that the pile head could only rotate or move together with the trusses. The horizontal loading point was 285 mm above the ground level. In order to verify the effectiveness of the half pile model, a whole single-pile model test was also conducted as a benchmark. As shown in Fig. 5, the whole

Accepted manuscript doi:
10.1680/jphmg.20.00030

single pile model was installed in the middle of the model container. The distance between the horizontal load application point and ground level is also 145 mm.

2.3 Loading schemes

All the tests were conducted under an equivalent centrifugal acceleration of 50g. The equivalent centrifugal acceleration was calculated based on the effective radius of the centrifuge machine, 2 m, which was 250 mm higher than the bottom of the model container. Considering the height of the models, the acceleration of the vertical loading point in test #2 was 38.8 g.

Five independent centrifuge model tests with different loading schemes were conducted in this study. Test #0 was a whole-pile pure lateral loading test that was used as a benchmark. Tests #1 and #2 were for lateral loading of single piles tests without and with constant vertical load, respectively. In test #1, only lateral load was applied onto the pile after the acceleration reached 50 g. In test #2, the steel pieces with a total mass of 1.02 kg were fixed onto the pile cap. The weights of the steel pieces increased by 38.8 times after the effective centrifuge acceleration reached 50 g, which provide a vertical load of 388 N at model scale. Test #2 aimed to simulate a typical load combination of piles for oil platforms or the monopiles for offshore wind turbines with a pre vertical load followed by horizontal loading. Tests #3 and #4 were lateral loading tripod-pile tests with opposite loading directions to simulate tripod-pile foundations for offshore wind turbines in different loading conditions. The half pile (Pile A) was compressed in test #3 and tensioned in test #4. In all the tests, the horizontal load was applied step by step with an interval of 20 N. Each step lasted for several minutes until the deformations of pile and soil became stable.

2.4 Measurement system

An image-capture and displacement measurement system was employed to measure the displacement of soil without disturbance to the model (Zhang et al. 2009). A high speed camera was installed in front of the model container to record the movements of pile and soil in the model container. White particles were applied to enhance the image contrast and achieve a measurement accuracy of 0.03 mm at model scale (Zhang et al. 2009). 13 pairs of strain gauges, with a foil size of 2mm×2mm and gauge resistance of 120 Ω, were attached onto the outer surface of each pile at different depths to derive bending moment along the piles. It should be noted that for half pile models, there was a 1-mm offset between the center of strain gauges and that of the model pile as it is a half cylinder. The resulting error has been verified by Lu and Zhang (2018) to be negligible. The strain gauges were connected in 1/4 bridges, so that the strain on each side of the bending section could be measured. During the post processing of the data, the measured strain, together with an intact pile cross section, was used to calculate the bending moment. Therefore, the results provided in this paper correspond to that of a whole pile. The effectiveness of measured bending moment will be further verified by comparing the results from half-pile and whole-pile tests. Besides, each strain gauge was covered by 1-mm-thick epoxy resin for protection, which may have some influences on the pile diameter

Accepted manuscript doi:
10.1680/jphmg.20.00030

and the shaft friction. However, due to the small size of the strain gauges, such influences were also assumed to be negligible in this study.

The results presented in this paper, including displacement, load and bending moment, have been transformed from model scale to prototype scale, which were calculated based on the effective centrifugal acceleration, 50 g. Leftward and downward are defined as positive for horizontal and vertical displacements, respectively. Compression is defined positive for the force, normal strain and normal stress. Anticlockwise is taken as positive for the bending moment.

2.5 Validation

The effectiveness of the half-pile model was first verified by comparing the results from the whole single-pile and half single-pile tests under pure lateral loading, which are test #0 and #1 respectively. It can be seen in Fig. 6 (a) that the pile deflection at the ground level from half and whole model tests match well under small horizontal load. The slightly stiffer behavior of the half pile under a larger horizontal load might be attributed to the friction between the half pile and the observation window, although silicon oil was used to reduce this potential friction. Nevertheless, the difference in pile deflection between the half-model and whole model is less than 10%, which is sufficiently small to be ignored.

The comparison of bending moments is shown in Fig. 6 (b), which shows a good agreement between half and whole model tests, except for a 12% decrease of the maximum bending moment in the half model test. As mentioned above, the decrease of bending moment in the half model test is because the strain gauges cannot be located at the central axis of the pile in the direction of bending. However, since the following comparisons of bending moment will only be conducted among half model tests, this error will not influence this comparative analysis. Besides, it can also be seen that the measured bending moments at the ground level are consistent with the theoretical value that is the product of the horizontal load (2 MN) and the distance from ground level to the load application point (7.5 m), which verifies the effectiveness of the measured bending moment.

3 OBSERVATIONS

3.1 Soil response

By tracing the movement of soil pixel points through the image-capture and displacement measurement system, the displacement vectors of the soil after loading could be calculated. Figs. 7 (a) and (b) show displacement vectors of the soil in single pile tests (tests #1 and #2). In the pure lateral loading test (test #1), a leftward movement of soil is significant near the ground level and decreases quickly with the increasing depth. Meanwhile, the lower part of the soil is almost motionless, indicating a flexible deformation of the pile. It can be seen that a downward movement occurs behind the pile near the ground level, which is because the sand flows into the gap that forms adjacent to the pile. For the density of the soil model, the modulus of subgrade reaction, n_h, is 10.7 MN/m^3 (Terzaghi 1955) and the Young modulus of aluminium, E, is 70 GPa. Thus, the characteristic length of the pile-soil system, $T = (EI/n_h)^{1/5} = 3.17$, and given that $L/T > 4$ verifies the pile is flexible (Matlock and Reese 1960). This behavior of sand

with a flexible pile under pure horizontal loading is different from that for rigid piles in clay (Zhang et al. 2013), where the pile displays a rigid rotation with the rotation center at the lower third of the pile length. In test #2, a static vertical load, representing gravity load, was first applied using steel pieces, and then horizontal loads was applied. It can be seen in Fig. 7 (b) that the soil beneath the pile tip is compressed, while soil around the pile, especially near the ground level, is dragged down by friction. Both of these downward movements may lead to an increase of soil density. Through further analyzing the vertical strain of soil under different vertical loading conditions, it has been proven by Lu and Zhang (2018) that the vertical load increased the confining pressure of the neighboring soil and correspondingly resulted in an increase in the soil stiffness, which was defined as ‘‘soil densification effect”. Therefore, as a result, the horizontal displacement of the soil under the same horizontal load in Fig. 7 (b) is smaller than that in pure lateral loading test in Fig. 7 (a). Besides, the maximum horizontal displacement of soil on the left side of the pile in test #2 moves from ground level to a lower position.

Figs. 7 (c) and (d) display the displacement vectors of the soil in tripod-pile tests under horizontal loads in opposite directions (tests #3 and #4). Contrary to single pile tests where the soil mainly exhibits horizontal displacement, downward or upward movements of the soil are observed in the tripod-pile foundation test. This is a result of load distribution in multi-pile foundations, which leads to transferring upper horizontal load to vertical- horizontal load combinations for the individual piles (Lu et al, 2016). In test #3 the horizontal load is leftward, and Pile A is compressed while undergoing bending. Larger rightward movements can be seen near the pile tip in Fig. 7 (c), which indicates a greater rigid rotation of the pile than that of single pile foundations. Conversely, the rightward load in test #4 sets Pile A in tension. It can be seen in Fig. 7 (d) that the soil on the right side is pulled up due to upward friction, while the soil on the left side flows downwards to the soil-pile gap. It is also observed that the horizontal displacements of the soil in test #4 are larger than those in test #3 under the same upper horizontal load. Besides, a larger rotation can be seen under the uplift-lateral load combination.

3.2 Displacements of piles

Fig. 8 shows the lateral load-displacement curves of pile at ground level in test #1-4. It should be noted that the pile lateral load shows here is the outer load applied on the superstructure, instead of the pile head load at the ground level. Generally speaking, the load-displacement responses for the single piles in Fig. 8 (a) are more linear than those of the tripod-pile foundations in Fig. 8 (b). And under the same horizontal load, the pile with pre vertical load (test #2) experiences less lateral deflection than that without vertical loading (test #1), which could be a result of soil densification effect. Similarly, it can be seen in Fig. 8 (b) that the deflection of Pile A in test #3 is less than that in test #4 because Pile A was under compression in test #3 while it was under tension in test #4. Besides, the load-displacement curve in test #4 obviously curves at the end of loading, probably indicating the occurrence of plasticity.

Accepted manuscript doi:
10.1680/jphmg.20.00030

The vertical displacement profile of piles under a certain horizontal load are shown in Figs. 9 (a)-(b). It can be seen in Fig. 9 (a) that there is no obvious vertical settlement or uplift of the single pile in the pure lateral loading test (test #1), whereas there is a slight downward movement of pile in test #2 due to the pre vertical compression. In contrast, as shown in Fig. 9 (b), there is a significant settlement of Pile A in test #3 and a twice larger uplift of Pile A in test #4. This result indicates that Pile A is compressed in test #3 while tensioned in test #4, which are the results of load distribution among multi-pile foundation under horizontal outer loading (Lu et al. 2016). Fig. 9 (c) shows the measured horizontal displacement profile of piles with depth in single pile tests. It can be observed that the pre vertical load decreases the lateral deflection of the pile. This may be attributed to the soil densification effect according to the above arguments. Although slight rightward movements are observed near pile tips in tests #1 and #2, flexible response is the dominant pattern for single pile foundations. Fig. 9 (d) shows the horizontal displacement of Pile A in tripod-pile tests. It is clear that the horizontal displacement under tension-bending combination is larger than that under compression and bending. It is reasonable to infer that the axial uplift on Pile A leads to an opposite influence to decrease the soil stiffness and increase the pile displacement correspondingly. Besides, owing to the soil-pile separation at the bottom, the pile tip constraint is weakened, and a greater rotation of the pile can be seen in test #4.

3.3 Bending moment of piles

Fig. 10 provides the measured bending moment of the piles under different load combinations. 6-order polynomial curve fitting was used to smooth the measured results. A nearly triangular distribution can be observed for all the piles. The maximum bending moments in single pile tests occur at 4-6 m deep while those in tripod-pile tests are lower. As shown in Fig. 10 (a-b), the bending moment of the single pile increases in the upper part with the presence of pre vertical load, but diminishes with depth. Similar results can be seen in tripod-pile tests (Fig. 10 (c-d)) where the bending moment of Pile A under compression is larger than that under tension. However, the difference between these two loading conditions continues with depth.

3.4 Shearing force of piles

By one-time differential of the curve-fitted bending moment profile, the shearing force profiles under different horizontal loads was calculated and presented in Fig 11. The shearing forces in test #1 and #2 are close to each other, except for an obviously larger result in test #2 at the pile tip. This is because the vertical load applied in test #2 increased the tip resistance, so that the shearing force was also enhanced. Besides, the shearing forces at the pile head are slightly larger than the applied horizontal load, which is a result of the uneven distribution of centrifugal acceleration. The shearing forces of pile A in the tripod-pile tests are shown in Figs. 11 (c) and (d). It can be seen that the distribution patterns of the shearing force of pile A under compression (test #3) and tension (test #4) are fairly different. The shearing force at the ground level in test #3 is 1.5-2 times larger than that in test #4, and the larger the horizontal load, the greater the difference. Besides, the minimum shearing force in the test #4 occurs at 12 m under both low and high horizontal loading level, but that in test #3 moves from 14 m to 10 m along

Accepted manuscript doi:
10.1680/jphmg.20.00030

with the increasing outer load. Furthermore, the shearing force at the pile tip in test #4 was almost zero because the pile-soil separation, meanwhile, that in test #3 is considerable. Based on the above observations, it can readily be concluded that the horizontal response of piles can be affected by different load combinations. In order to provide a more reliable design method, *p-y* curves of the piles under different combined loads should be further analyzed.

4 COMPUTATIONS of *p-y* CURVES

In this section, a computation process of *p-y* curves of the pile is presented based on the data of pure lateral loading test (test #1). The results are compared with two established *p-y* curve models.

According to Winkler elastic foundation beam theory, the relationships between lateral pressure, *p*, bending moment, *M*, and horizontal deflection, *y*, can be described by the following equations:

$$y(Z) = \frac{1}{EI}\iint M(Z)dZ \qquad (1)$$

$$p(Z) = \frac{d^2M(Z)}{dZ^2} \qquad (2)$$

Based on the bending moment derived from strain gauges and boundary conditions, values of *y* can be computed by double-integration with a satisfactory accuracy. The displacements can also be directly measured using the image-based analysis in this study. However, the earth pressure *p* is difficult to obtain due to the inaccuracies resulting from double differentiation. In this study, polynomial curve fitting was used to obtain smoother vertical distributions of bending moment and to derive earth pressure. The following section describes the implemented procedure.

4.1 Computation of horizontal displacements

The measured horizontal displacements of the pile in test #1 and those from double-integration of bending moments are compared in Fig. 12 for different horizontal forces. The known displacements of the pile at the ground level and the pile tip were taken as two boundary conditions for double-integration using Eq. (1). It can be seen that the results come from the two methods are in very good agreement. This agreement confirms both the validity of the beam theory and the accuracy of the image measurement system used in this study. Therefore, measured horizontal displacements are used to develop *p-y* curves in the following analyses. A mild curve fitting was used to make the measured pile deflection curves smoother.

4.2 Computation of earth pressure

Fifth, sixth and seventh order polynomials were used for fitting the bending moment variation and calculating the earth pressure using double-differentiation. The boundary condition of zero earth pressure at ground level was applied to ensure a more realistic fit. Fig. 13 displays the earth pressure with different orders of polynomial fitting together with that from

double-differentiation of measured bending moments. According to the observation in Fig. 9, there is a slight rotation of pure lateral loading pile. Thus, the distribution of earth pressure derives from 5-order polynomial with a zero or minus value at the pile tip is unrealistic. The results from 6- and 7-order polynomial fitting are fairly similar except close to the pile tip. The 6-order polynomial provides a better match with the measured data close to the pile tip, which was discovered in previous centrifuge studies (Klinkvort and Hededal 2014; Zhu et al. 2014). Therefore, 6-order polynomial curve fitting was selected for derivation of the earth pressures and computation of the *p-y* curves in this study.

4.3 p-y curves for pure lateral loading test

Based on the methods described above, *p-y* curves in pure lateral loading test (test #1) were computed and are presented in Fig. 14. It can be seen that the initial stiffness of the curves increases with depth except at 7 m depth near the rotation center of the pile where both *p* and *y* have very low values. Fig. 15 compares the *p-y* curves from the test to those suggested by the American Petroleum Institute (API 2000) design code. As seen in these plots, the initial stiffnesses of API *p-y* curves are considerably larger than those from the test. Also, the *p-y* curves obtained from test #1 are a hardening type without a yielding stage, which is also different from the hyperbolic tangential *p-y* curve of the API code. Similar *p-y* curves with larger initial stiffness and no yielding stage were also obtained by Klinkvort and Hededal (2014) and Zhu et al (2014) from monopile and jacket-pile centrifuge model tests.
Recent studies have demonstrated that a hyperbolic *p-y* curve is more realistic to describe the lateral response of soil-pile system with the following equation (Dewaikar and Patil 2006; Klinkvort and Hededal 2014; Zhu et al. 2014):

$$p = \frac{y}{\frac{1}{k_{ini}} + \frac{y}{p_u}} \qquad (3)$$

where k_{ini} is the initial modulus, p_{u} is the ultimate lateral bearing capacity of soil base. According to previous research and test data the following nonlinear correlation was proposed between initial modulus k_{ini} and depth:

$$k_{ini} = n_h Z^{\alpha} \qquad (4)$$

Using the data in this study, the initial modulus coefficient, n_{h}, is taken as 2000 kN/m^3, and α is taken as 0.5. The power 0.5 is consistent with earlier studies on the variation of shear modulus with depth (Kramer 1996). In order to fit the test data, the API equation of ultimate lateral bearing capacity, p_{u}, for sand for large depth is used:

$$p_{ud} = C_3 D \gamma Z \qquad (5)$$

where $C_3 = 100$. The calculated *p-y* curves using hyperbolic *p-y* model are also shown in Fig. 15. It can be seen that hyperbolic model better represents the test results than the API *p-y* curves.

Accepted manuscript doi:
10.1680/jphmg.20.00030

5 *p-y* CURVES FOR COMBINED LOADS

p-y curves of the piles in the different tests were calculated using the above process. The results were compared to highlight the influence of different load combinations on the lateral response of soil-pile systems.

5.1 Single-pile tests

Fig. 16 compares the *p-y* curves in pure lateral loading test (test #1) and in combined loading test (test #2) of single piles. It is observed that the soil after vertical loading exhibits a higher resistance, which may be a result of soil densification. Such a result implies that self-weight of superstructures of oil platform or offshore wind turbines plays a positive role in increasing the lateral resistance of the soil neighboring the pile.

5.2 Tripod-pile tests

Fig. 17 shows the *p-y* curves of Pile A in tripod-pile foundation under different loading directions (test #3 and #4). The results of the pure lateral loading test (test #1) are also included for comparison. Contrary to the single pile test under combined loads where the vertical load was constant during application of the horizontal load, the axial and lateral loads on Pile A in tripod-pile foundation increase simultaneously. The *p-y* curves for the tripod-pile foundations exhibit more linear trends. Compared with the *p-y* curves of pure lateral loading test, the *p-y* curves of the compressed-bending pile are stiffer due to the effect of soil densification, while the *p-y* curves of the pile in tension and bending are softer due to the opposite phenomenon. The observations of tripod-pile tests are in good agreement with the results of previous centrifuge model tests on jacket-pile foundation (Zhu et al. 2014) that the *p-y* curves for compressed pile are stiffer than those in tension.

Based on these test results, it is clear that *p-y* curves are influenced by vertical loads. Therefore, the current *p-y* curves used by the industry need to be re-evaluated for acceptable reliability.

6 OBSERVATIONS RELATED TO DESIGN

On the basis of forgoing analyses of the centrifuge tests data (Lu and Zhang 2018), it is observed that two sides of influences of vertical load on the lateral behavior of soil-pile systems should be taken into consideration: on one hand, the axial force tends to de nsify or loosen the soil and change the *p-y* curves; on the other hand, it leads to additio nal bending moments due to *P*-Δ effect. The interplay of these two mechanisms makes t he lateral behavior of piles under combined loads to be different from that under pure la teral load. However, the current design method for combined loading of piles only takes *P*-Δ effect into account by including the secondary effect of axial load into the differenti al equation of horizontal pile response on springs as follows (Zhang et al. 2011):

$$EI\frac{d^4Y(Z)}{dZ^4}+F_{axial}(Z)\frac{d^2Y(Z)}{dZ^2}=kY(Z) \qquad (6)$$

Accepted manuscript doi:
10.1680/jphmg.20.00030

where F_{axial} is the axial force along the pile. In order to evaluate the current design method, different *p-y* curves with the loading conditions of test #1 (V=0MN) and #2 (V=2.5MN) were used to back-calculate pile responses and to compare with measured data.

6.1 Pile response by different models

It is known that the reliability of *p-y* curves derived from model tests are affected by different kinds of errors, such as the error from measurement system, the error due to scale effect, and the error from double differentiation of bending moment (Klinkvort and Hededal.2016; Zhu et al. 2014). In this study, no parallel tests were available to either support the effectiveness of the *p-y* curves or provide the error bars of each point. Therefore, indirect verification method was employed, which is to back calculate the pile lateral responses using the calculated *p-y* curves, to verify the effectiveness of the derived *p-y* curves.

Figs. 18 (a) and (b) show the back-computed displacement and bending moment using API *p-y* curves for drained sand where the axial force F_{axial} was assumed constant along depth. Comparing the results of pure laterally loaded pile (the circles and the solid curves), it is observed that the displacements by API *p-y* curves are smaller than those measured. This is expected due to the stiffer *p-y* curves in API (Fig. 15). The same mechanism explains the larger moments close to the ground surface and smaller moments at larger depth using the API curves. Nevertheless, from a practical viewpoint, it is interesting to note that despite the considerably larger stiffness of API *p-y* curves, the pile responses are not dramatically different than the measured values. The figure also displays the pair of results (measured and computed) for the cases with and without the axial load. These results indicate the significance of consideration of P-Δ effect on both displacement and bending moment.

To ascertain the accuracy of the simplified hyperbolic *p-y* curves, the calibrated hyperbolic curves of test #1 (with n_h= 2 MN/m^3, α=0.5 and C_3=100) and test #2 (with n_h=3.7 MN/m^3, α=0.5 and C_3=100), were used to compute the pile responses in the two tests. The results are shown together with the measured data in Figs. 18 (c) and (d). The back-calculated results agree well with the measured data except for a slight deviation of the lateral deflection of the pile tip in test #1, which might be attributed to the errors from the measurement and the post-processing (such as differentiation) of the test data. Since the lateral deflection of the pile tip is less significant compared to that of pile head, the authors decided to sacrifice the precision here for the best agreements at other parts. Apart from the slight deviation, the good agreements of pile deflections and bending moments indicate the accuracy of the calibration and computation process of *p-y* curves from the tests. Moreover, a higher n_h reflects the soil densification for compression-bending combined loading condition; this supports that both the change of *p-y* curves and P-Δ effect due to vertical load should be taken into consideration.

The response of the pile head was also computed as a function of the lateral load using API *p-y* curves and compared with the test results in Fig. 19 (a). It can be observed that while the API *p-y* curves underestimate the pile-head displacement at small horizontal loads, as explained earlier, they overestimate the pile-head displacement at larger loads because of their lower capacities compared to the measured *p-y* curves (Fig. 15). By ignoring densification, the

difference between pure lateral loading and combined loading tests is only from the *P*-Δ effect. This is in contrast to the measured data. On the contrary, the results from hyperbolic *p-y* curves fit well with the measured data in Fig. 19 (b), which again highlights the dependency of *p-y* curves on vertical loads.

6.2 Initial stiffness of p-y curves

It has been revealed in this study that vertical loading increases the stiffness of soil neighboring the pile. Therefore, it is fair to infer that during pile jacking in the field there will also be a soil densification effect and an increase of soil stiffness. It should be noted that, by installing the pile under 1 g with a much lower stress level, the soil densification effect was greatly reduced, which might also influence the initial soil resistance. That was speculated to be a possible reason that the initial stiffness of *p-y* curves in this study is smaller than commonly encountered. However, the installation effects were eliminated during comparison because all the piles were installed in the same way. The installation effect might influence the shape of *p-y* curves, but it did not change the core discovery in this study that vertical compression enhances the *p-y* curves while vertical tension decreases the *p-y* curve.

7 SUMMARY AND CONCLUSIONS

In this study, two single pile tests and two tripod-pile tests were used to investigate the influence of combined loads on the lateral response of soil-pile systems. The displacement and the bending moment were measured and analyzed to highlight the behavior of pile-soil systems under different loading conditions. A calculation process of *p-y* curves was developed based on the data of pure lateral loading test. Then *p-y* curves in different tests were compared to highlight the influence of combined loads on the lateral behavior of soil-pile systems. The following conclusions have been drawn:

(1) The axial compression tends to densify the soil and increase the soil stiffness. Thus, the *p-y* curves of a compressed-bending pile have a stiffer response than those of a pure laterally loaded pile. This indicates that self-weight of the superstructure plays a positive role to increase the soil lateral resistance.

(2) The axial tension, on the other hand, has an opposite influence. The *p-y* curves of tensioned-bending pile are softer than those of pure lateral loading pile. Therefore, more attention should be paid to the design of multi-pile foundations for offshore wind turbines for uplift conditions.

(3) The *p-y* curves derived in this study are hardening type, with lower initial stiffness and larger ultimate resistance compared with those from API. It is found that a hyperbolic model can better represent the test results than the API *p-y* curves.

(4) Both the change of *p-y* curves and the *P*-Δ effect due to vertical load should be taken into consideration for the design of piles under vertical-horizontal combined loads.

(5) The drainage condition of sand is an important parameter in response of piles and could have a major influence on the natural frequency of the pile-soil-structure system.

ACKNOWLEDGEMENTS

The study is supported by National Key R&D Program of China (2018YFC1508503) and the Norwegian Research Council (No. 243984).

NOTATIONS

D	Diameter of the pile
EI	Bending stiffness of the pile cross section
H	Horizontal load
k_{ini}	Initial stiffness of the *p-y* curve
L	Buried length of the pile
M	Bending moment of the pile
p	Lateral resistance of soil
p_u	Ultimate lateral resistance of soil
V	Vertical load
y	lateral deflection of the pile
Z	Depth below the ground level
γ	Soil unit weight

REFERENCES

[1] American Petroleum Institute (API). Recommended Practice for Planning, Designing and Constructing Fixed Offshore Platforms-Working Stress Design, twenty-frst ed. API Recommended Practice 2A-WSD (RP2A-WSD), 2000, Dallas.

[2] Achmus, M., Abdel-Rahman, K., Thieken, K. Behavior of piles in sand subjected to inclined loads. In Proceedings of the 1st International Symposium on Computational Geomechanics (ComGeo I), Juan-les-Pins, France, 2009, p. 763–774.

[3] Byrne B., McAdam, R., Burd, H., Houlsby, G., Martin, C., Beuckelaer, W., Zdravkovic, L., Taborda, D., Potts, D. and Jardine, R. PISA: new design methods for offshore wind turbine monopiles. Proc. 8th Intl. Conf. Offshore Site Investigation and Geotechnics, London, UK, 2017, 142-161

[4] Chatterjee, K., Choudhury, D. Analytical and numerical approaches to compute the influence of vertical load on lateral response of single pile. Japanese Geotechnical Society Special Publication 2015; 2:1319-1322.

[5] Darr, K. A., Reese, L. C., Wang, S. T. Coupling effects of uplift loading and lateral loading on capacity of piles. In Offshore Technology Conf., British Maritime technology, Teddington, 1990, p. 443–450.

[6] Dewaikar D. M., Patil P. A. A new hyperbolic p-y curve model for laterally loaded piles in soft clay. In Geoshanghai International Conference, Shanghai, 2006, p. 152-158.

[7] Ismael, N. F. Field tests on bored piles subject to axial and oblique pull. J. Geotech. Eng 1989; 11(1588): 1588–1598.

[8] Jeanjean P., Zhang, Y., Zakeri, A., Andersen, K., Gilbert, R. and Senanayake, A. A framework for monotonic py curves in clays. Proc. 8th Intl. Conf. Offshore Site Investigation and Geotechnics, London, UK, 2017, 108-141

[9] Karasev O. V., Talanov G. P., Benda S. F. Investigation of the work of single situ-cast piles under different load combinations. Soil Mech. Found. Eng. 1977; 3: 73–177.

[10] Karthigeyan S., Ramakrishna V.V.G.S.T. and Rajagopal K. Influence of vertical load on the lateral response of piles in sand. Comput. Geotech. 2006; 33: 121–131.

[11] Klinkvort, R. T., Hededal, O. Effect of load eccentricity and stress level on monopile support for offshore wind turbines. J. Geotech. Eng. 2014; 10(4): 50–58.

[12] Kramer, S.L. Geotechnical Earthquake Engineering. Prentice-Hall Inc., New Jersey, 1996.

[13] Lee J., Prezzi M., Salgado R. Experimental investigation of the combined load response of model piles driven in sand. Geotechnical Testing Journal 2011; 34: 653–667.

[14] Lu W.J., Zhang G., Wang A.X. Bearing behavior of multiple piles for offshore wind driven generator. Ocean Engineering 2016; 129: 538-538.

[15] Lu W.J., Zhang G. Influence mechanism of vertical-horizontal combined loads on the response of a pile in sand. Soils and Foundations 2018; 58 (5): 1228-1239.

[16] Matlock H., Reese L. C. Generalized Solutions for Laterally Loaded Piles. Journal of the Soil Mechanics and Foundations Division, 1960; 86 (15): 63-92.

[17] Matlock H. Soil Modulus for laterally loaded piles. Journal of the Soil Offshore Technology in Civil Engineering 1970; 77-94.

[18] Madhav M. R., Sarma C. P. K. Analysis of axially and laterally loaded long pile. In Proceedings of the Second International Conference on Numerical Methods in Offshore Piling, Institution of Civil Engineers (ICE), Austin, TX, 1982, p. 577–596.

[19] Mroueh, H., Shahrour, I. Response of piles to inclined uplift load: Influence of the soil-pile interface. Eur. J. Comput. Mech. 2007; 16(3–4): 419–436.

[20] Poulos H. G., Davis E. H. Pile foundation analysis and design. New York, Wiley, 1980.

[21] Reddy A., Ramasamy G. Analysis of an axially and laterally loaded tapered pile in sand. Soils Found. 1973; 13(4): 15–27.

[22] Reese L. C., Cox W. R., Koop F. D. Analysis of laterally loaded piles in sand. Offshore Technology in Civil Engineering 1974; 95-105.

[23] Romo M. P., Ovando-Shelley E. P–y curves for piles under seismic lateral loads. Journal of Geotechnical & Geoenvironmental Engineering 1998; 16(4): 251-272.

[24] Reddy K M, Ayothiraman R. Experimental studies on behavior of single pile under combined uplift and lateral loading. Journal of Geotechnical & Geoenvironmental Engineering 2015; 141(7): 04015030.

[25] Sorochan E. A., Bykov V. I. Performance of groups of cast in place piles subjected to horizontal loading. J. Soil Mech. Found. Eng. 1976; 13(3): 157–161.

[26] Stevens, J. B., Audibert, J. M. E. Re-examination of p-y curve formulations. Offshore Technology Conf., Houston, 1979: 397–403.

[27] Terzaghi, K. Evaluation of coefficients of subgrade modulus. Geotechnique 1955; 5(4): 297-326.

[28] Zhukov N. V., Balov I. L. Investigation of the effect of a vertical surcharge on horizontal displacements and resistance of pile columns to horizontal loads. Soil Mech. Found. Eng. 1978; 1: 16–21.

[29] Zhang, L. Y., Chen, Z. C. A new p-y curve construction method in cohesive soil. Ocean Eng. 1992; 10(4): 50–58. (in Chinese)

[30] Zhang G., Hu Y., Zhang J.M. New image analysis-based displacement-measurement system for geotechnical centrifuge modeling tests. Measurement 2009; 42: 87–96.

[31] Zhang L., Gong X. N., Yang A. X., Yu J. L. Elastoplastic solutions for single piles under combined vertical and lateral loads. Journal of Central South University of Technology 2011; 18(1): 216-222.

[32] Zhang G., Rong B., Fu P. Centrifuge model test study of static and cyclic behavior of a pile foundation for an offshore wind generator. Journal of Testing and Evaluation 2013; 41: 701-712.

[33] Zhu B., Li T., Bi M J. Centrifuge modelling on tetrapod jacket foundation subjected to lateral loads. Chinese J. Geotech. Eng. 2014; 36: 1822-1830. (in Chinese)

[34] Zhao C., Liu F., Qiu Z., Zhao C., Wang W. Study on bearing behavior of a single pile under combined vertical and lateral loads in sand. Chinese Journal of Geotechnical Engineering 2015; 37(1): 183–190. (in Chinese)

Accepted manuscript doi:
10.1680/jphmg.20.00030

Table 1 Property parameters of sand

Relative density	0.58
Effective particle size (D_{10})	0.107 mm
Mean particle size (D_{50})	0.192 mm
Coefficient of Curvature (C_c)	1.106
Coefficient of Uniformity (C_u)	2.149
Maximum void ratio	0.78
Minimum void ratio	0.47
Effective friction angle (φ')	32°

Table 2 Initial stiffness of *p-y* springs from different methods

Z/D	**$k_{test\#1}$ (MPa)**	**$k_{test\#2}$ (MPa)**	**k_{API} (MPa)**	**$k_{drained}$ (MPa)**	**$k_{undrained}$ (MPa)**
1	2	3.7	11	68	3.3
2	3	5.2	22	96	6
3	3.4	6.4	33	118	8
4	4	7.4	44	136	10
5.5	4.7	8.7	60	160	13
7	5.3	9.8	77	180	16
14.5	7.6	14	160	259	28
16	8	15	176	272	31

Accepted manuscript doi:
10.1680/jphmg.20.00030

Figure captions

Fig. 1 Grain-size distribution curve of the silica sand used in this study.

Fig. 2 Schematic diagram of the vacuum saturation system.

Fig. 3 Schematic view of the haft single pile in tests #1 and #2 under combination loads (unit: mm). (a) elevation view; (b) plan view; (c) photo.

Fig. 4 Schematic view of the tripod-pile in tests #3 and #4 under horizontal load (unit: mm). (a) elevation view; (b) plan view; (c) photo.

Fig. 5 Schematic view of the whole single pile in tests #0 under horizontal load (unit: mm). (a) elevation view; (b) plan view; (c) photo.

Fig. 6 Comparisons of the lateral displacement and bending moment between half and whole pile test under pure horizontal loading. (a) lateral load-displacement curve at the ground level; (b) bending moment. *Z*, depth; *H*, horizontal load.

Fig. 7 Displacement vectors of the soil in vertical plane. (a) single pile test #1; (b) single pile test #2; (c) tripod-pile test #3; (d) tripod-pile test #4. *Z*, depth; *X*, horizontal coordination.

Fig. 8 Lateral load-displacement curves of pile at ground level in test #1-4. (a) single pile tests; (b) tripod-pile tests.

Fig. 9 Profiles of the measured horizontal and vertical displacements of the pile under different loading conditions (a) vertical displacement in single-pile tests; (b) vertical displacement tripod-pile tests; (c) horizontal displacement in single-pile tests; (d) horizontal displacement tripod-pile tests. *Z*, depth; *H*, horizontal load.

Fig. 10 Profiles of pile bending moment under different loading conditions (a) *H*=0.75 MN in single-pile tests; (b) *H*=2 MN in single-pile tests; (c) *H*=2.5 MN tripod-pile tests; (d) *H*=4.5 MN tripod-pile tests. *Z*, depth; *H*, horizontal load.

Fig. 11 Profiles of pile shearing force under different loading conditions. (a) *H*=0.75 MN in singlepile tests; (b) *H*=2 MN in single-pile tests; (c) *H*=2.5MN tripod-pile tests; (d) *H*=4.5 MN tripod-pile tests. *Z*, depth; *H*, horizontal load.

Fig. 12 Comparisons of horizontal displacement of the pile from different methods in test #1 for different horizontal forces. (a) *H*=0.5 MN; (b) *H*=1.3 MN. *Z*, depth; *D*, pile diameter; *H*, horizontal load.

Fig. 13 Comparisons of earth pressure from different orders of polynomial curve fitting under different horizontal loads in test #1 for different horizontal forces. (a) *H*=0.25 MN; (b) *H*=1 MN; (c) *H*=1.5 MN; (d) *H*=2 MN. *Z*, depth; *D*, pile diameter; *H*, horizontal load; *p*, earth pressure.

Fig. 14 *p*-*y* curves in pure lateral loading test at different depths. *Z*, depth; *D*, pile diameter; *p*, earth pressure; *y*, horizontal displacement.

Fig. 15 Comparisons of *p-y* curves from pure lateral loading test with those from API for drained assumption and hyperbolic model at different depths. (a) *Z*/*D*=2; (b) *Z*/*D*=4; (c) *Z*/*D*=7; (d) *Z*/*D*=14.5. *Z*, depth; *D*, pile diameter; *p*, earth pressure; *y*, horizontal displacement.

Fig. 16 Comparison of *p-y* curves for different loading conditions in single-pile tests at different depths. (a) *Z*/*D*=1; (b) *Z*/*D*=2; (c) *Z*/*D*=4; (d) *Z*/*D*=14.5. *Z*, depth; *D*, pile diameter; *p*, earth pressure; *y*, horizontal displacement.

Fig. 17 Comparison of *p-y* curves for different loading conditions in tripod-pile tests at different depths. (a) *Z*/*D*=1; (b) *Z*/*D*=2; (c) *Z*/*D*=5.5; (d) *Z*/*D*=14.5. *Z*, depth; *D*, pile diameter; *p*, earth pressure; *y*, horizontal displacement.

Fig. 18 Comparisons of back-calculated lateral responses of the pile from different *p-y* curves to test data. (a) lateral displacement by API *p-y* curves; (b) bending moment by API *p-y* curves; (c) lateral displacement by Hyperbolic *p-y* curves; (d) bending moment by Hyperbolic *p-y* curves. *Z*, depth; *H*, horizontal load; *V*, vertical load; *y*, horizontal displacement.

Fig. 19 Comparisons of back-calculated lateral displacement of pile at ground level from different *p-y* curves to test data. (a) from API *p-y* curve; (b) from Hyperbolic *p-y* curve. *H*, horizontal load; *V*, vertical load; *y*, horizontal displacement.

Accepted manuscript doi:
10.1680/jphmg.20.00030

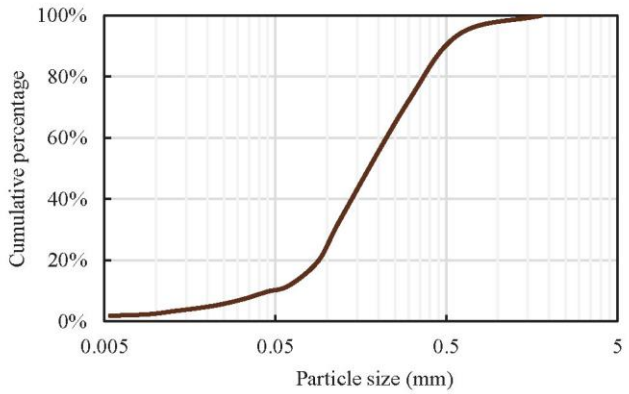

FIG. 1 Grain-size distribution curve of the silica sand used in this study.

Accepted manuscript doi:
10.1680/jphmg.20.00030

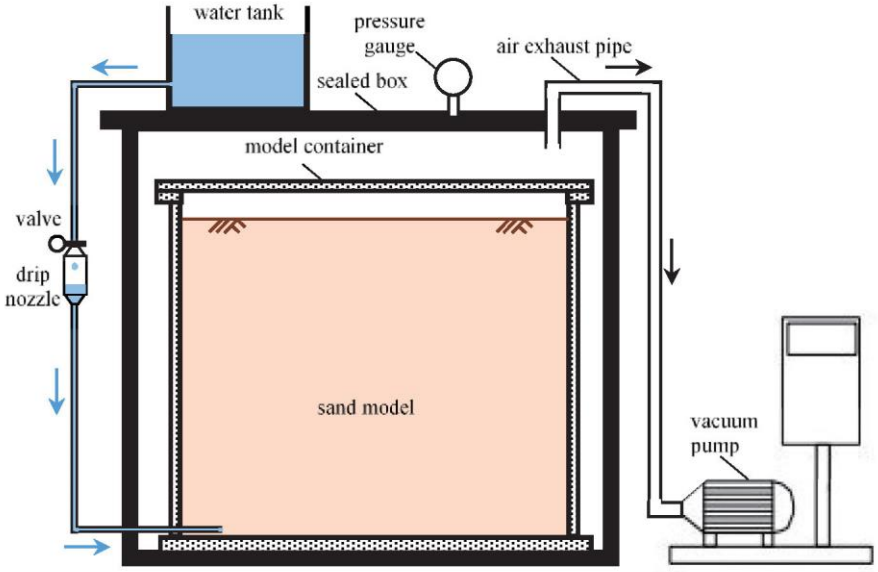

FIG. 2 Schematic diagram of the vacuum saturation system.

Accepted manuscript doi:
10.1680/jphmg.20.00030

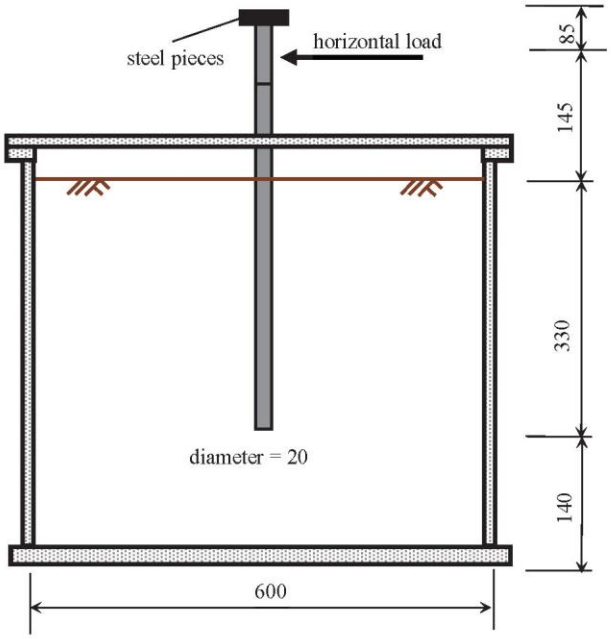

(a)

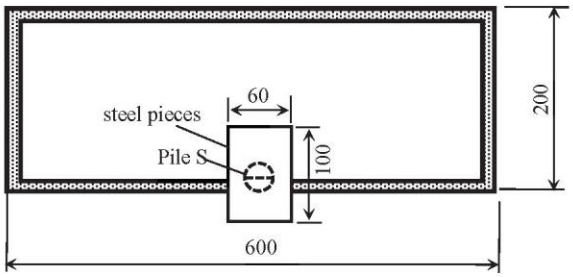

(b)

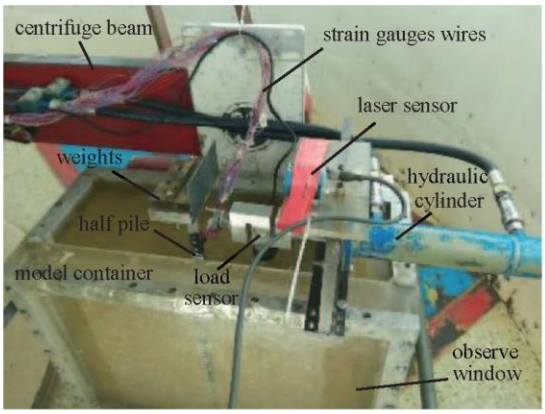

(c)

FIG. 3 Schematic view of the haft single pile in tests #1 and #2 under combination loads (unit: mm). (a) elevation view; (b) plan view; (c) photo.

Accepted manuscript doi:
10.1680/jphmg.20.00030

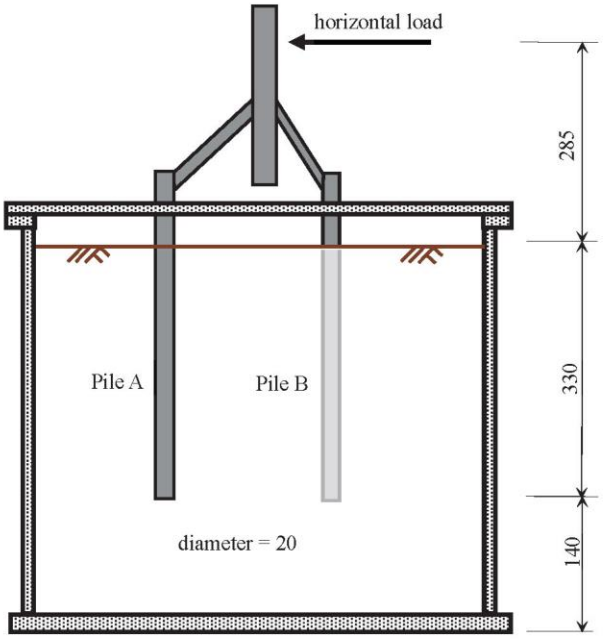

(a)

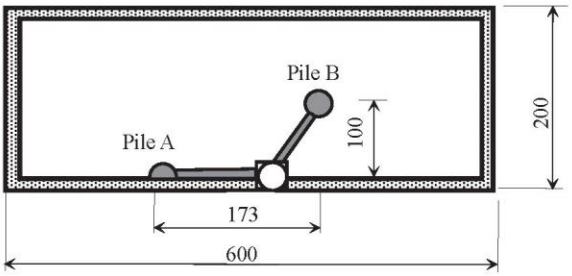

(b)

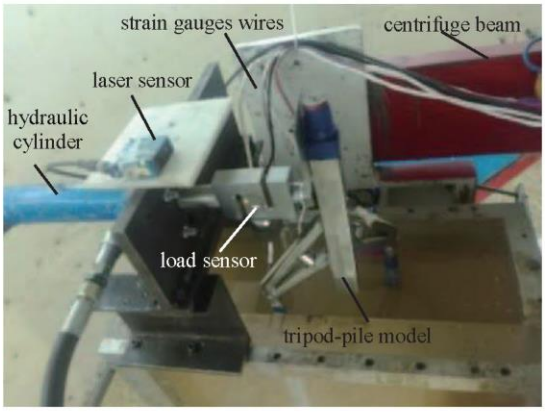

(c)

FIG. 4 Schematic view of the tripod-pile in tests #3 and #4 under horizontal load (unit: mm). (a) elevation view; (b) plan view; (c) photo.

Accepted manuscript doi:
10.1680/jphmg.20.00030

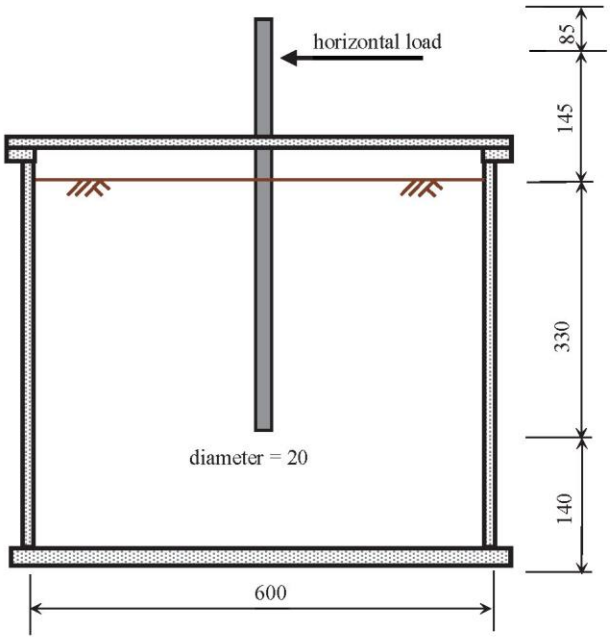

(a)

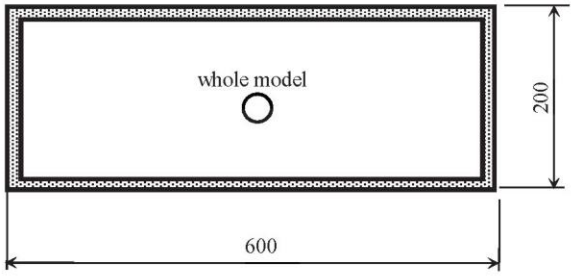

(b)

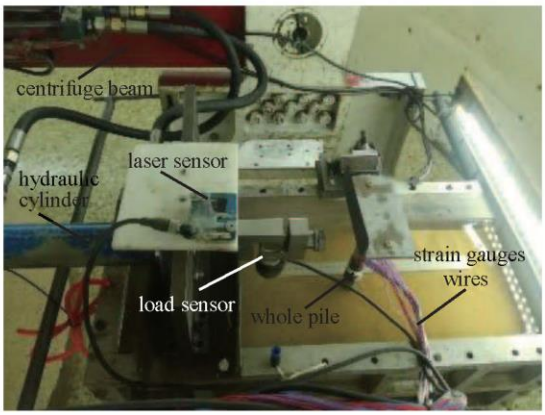

(c)

FIG. 5 Schematic view of the whole single pile in tests #0 under horizontal load (unit: mm). (a) elevation view; (b) plan view; (c) photo.

Accepted manuscript doi:
10.1680/jphmg.20.00030

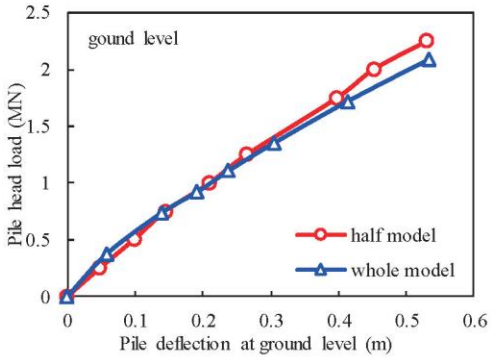

(a)

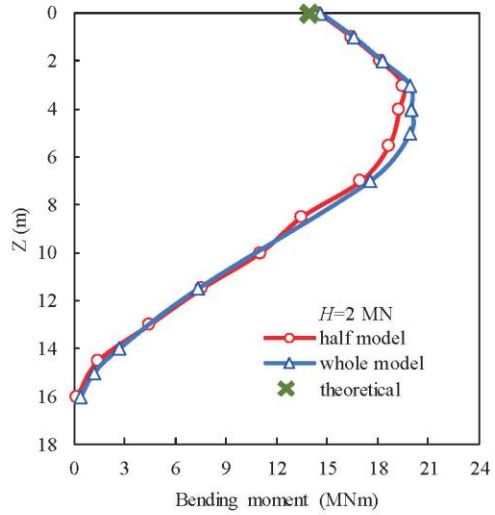

(b)

FIG. 6 Comparisons of the lateral displacement and bending moment between half and whole pile test under pure horizontal loading. (a) lateral load-displacement curve at the ground level; (b) bending moment. Z, depth; H, horizontal load.

Accepted manuscript doi:
10.1680/jphmg.20.00030

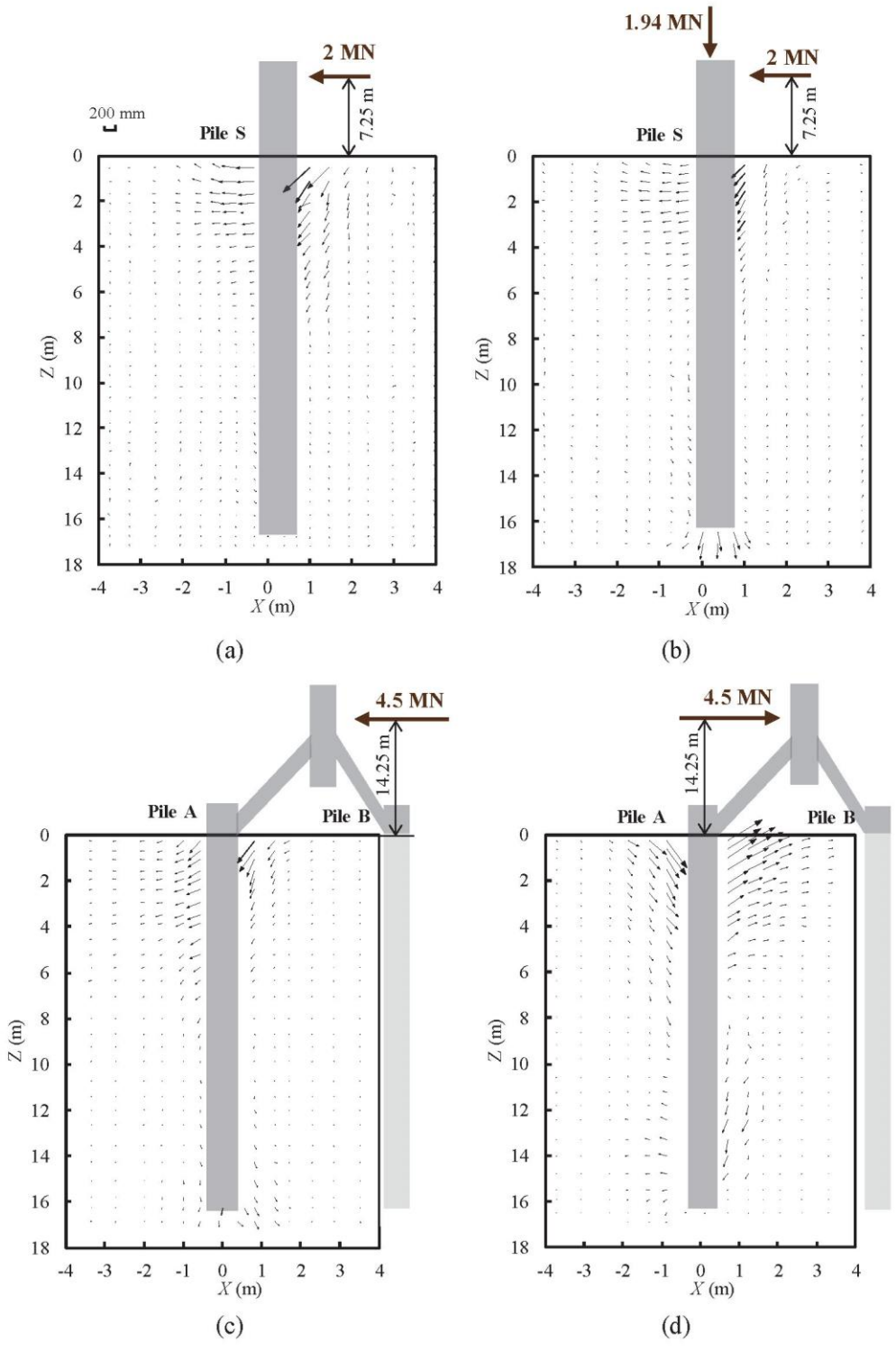

FIG. 7 Displacement vectors of the soil in vertical plane. (a) single pile test #1; (b) single pile test #2; (c) tripod-pile test #3; (d) tripod-pile test #4. *Z*, depth; *X*, horizontal coordination.

Accepted manuscript doi:
10.1680/jphmg.20.00030

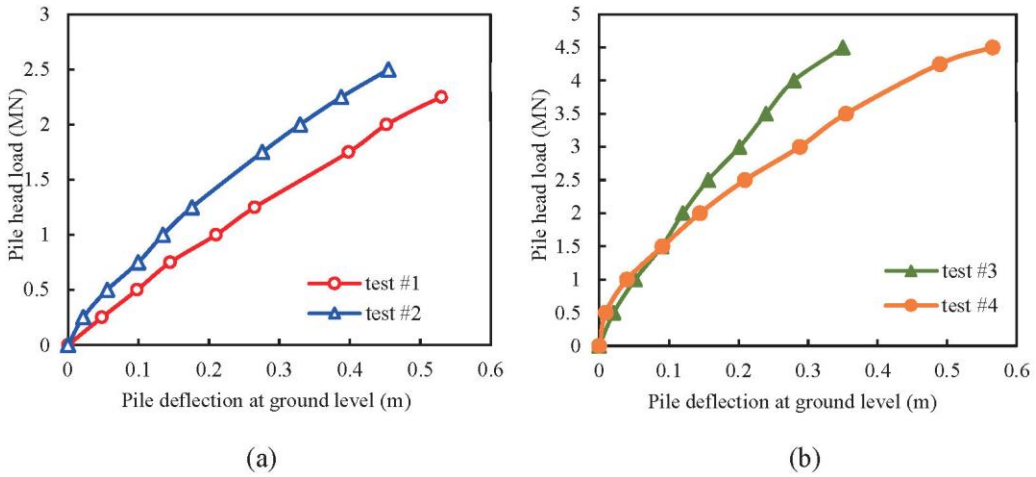

FIG. 8 Lateral load-displacement curves of pile at ground level in test #1-4. (a) single pile tests; (b) tripod-pile tests.

Accepted manuscript doi:
10.1680/jphmg.20.00030

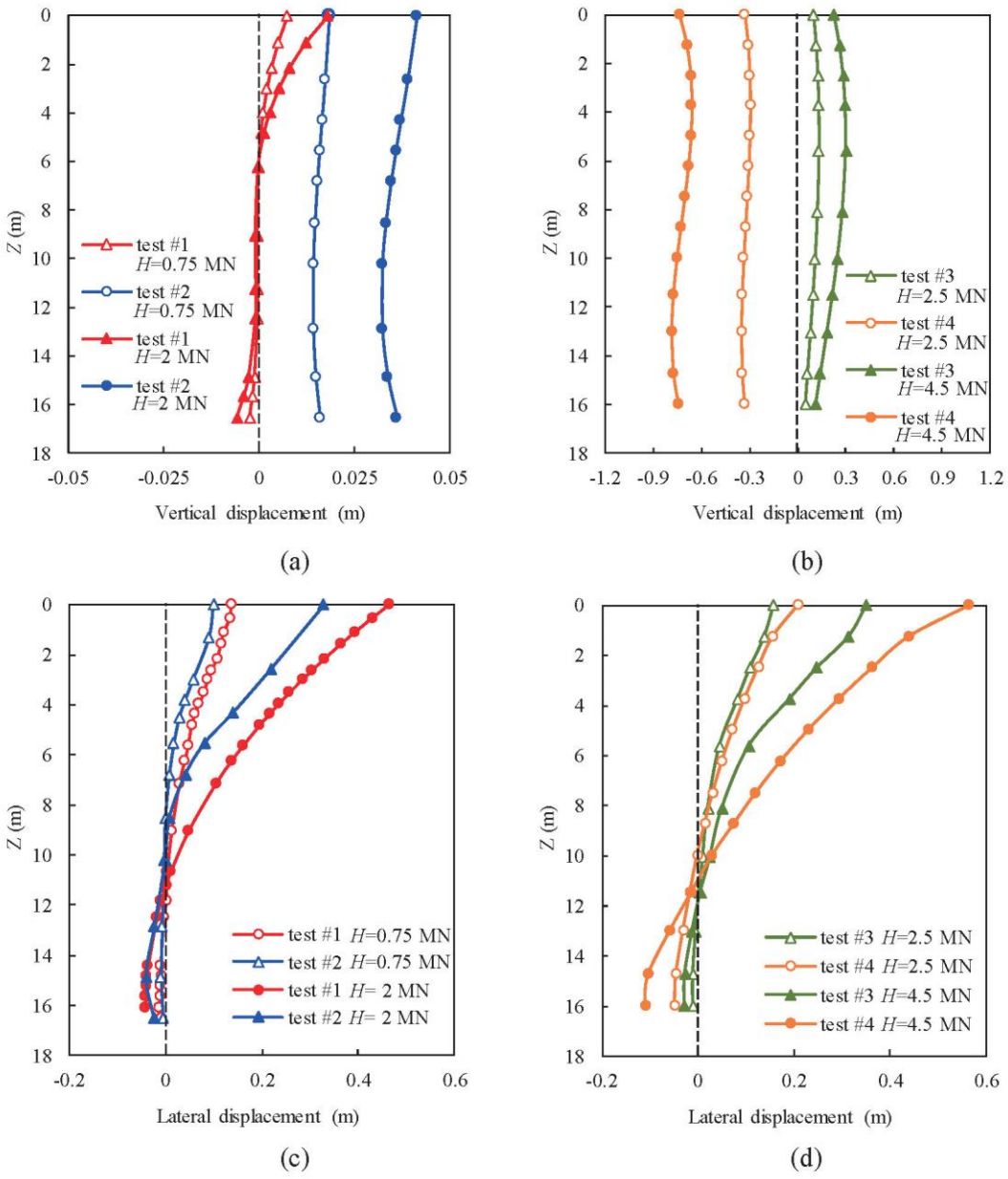

FIG. 9 Profiles of the measured horizontal and vertical displacements of the pile under different loading conditions (a) vertical displacement in single-pile tests; (b) vertical displacement tripod-pile tests; (c) horizontal displacement in single-pile tests; (d) horizontal displacement tripod-pile tests. *Z*, depth; *H*, horizontal load.

Accepted manuscript doi:
10.1680/jphmg.20.00030

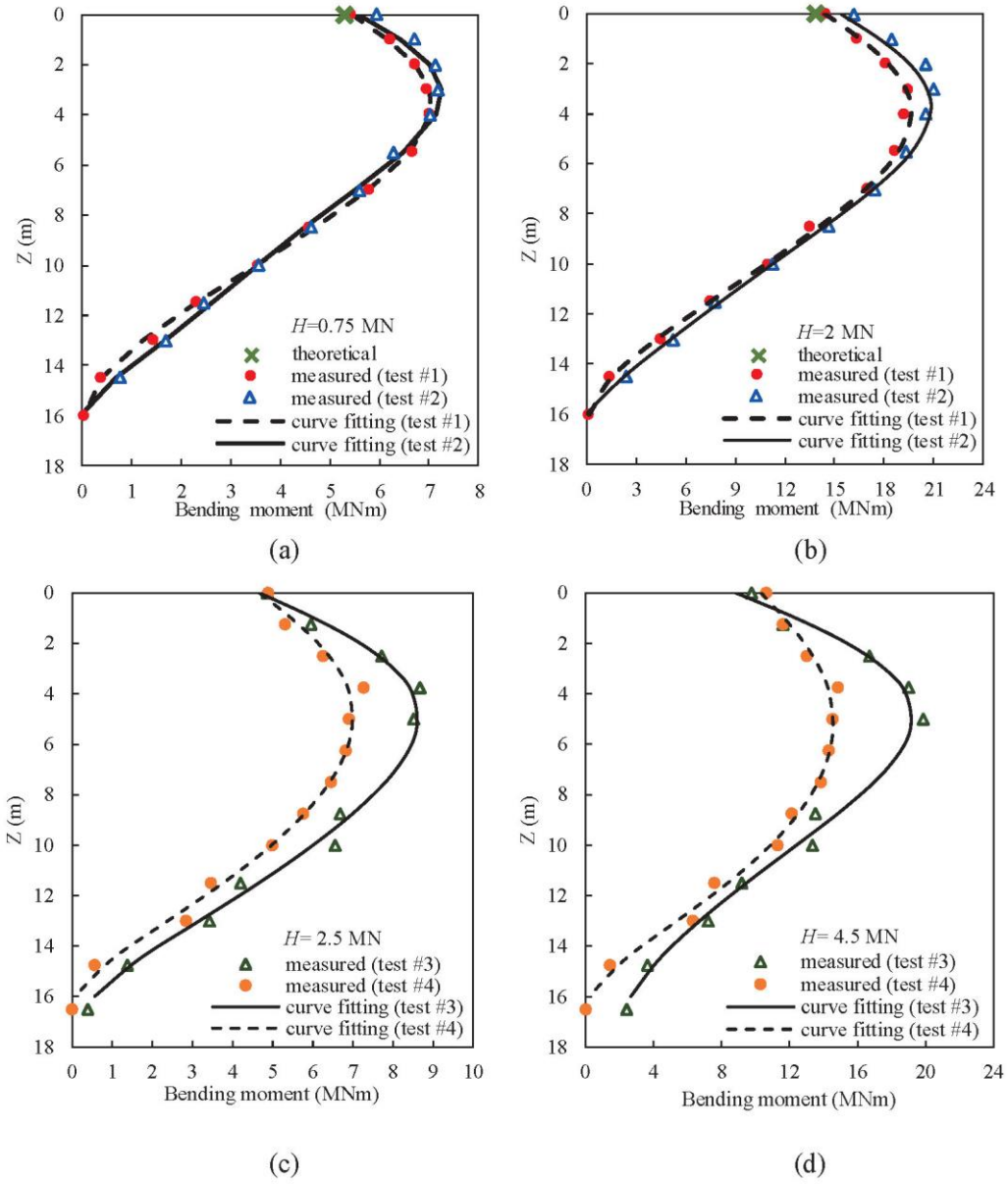

FIG. 10 Profiles of pile bending moment under different loading conditions(a) H=0.75 MN in single-pile tests; (b) H=2 MN in single-pile tests; (c) H=2.5 MN tripod-pile tests; (d) H=4.5 MN tripod-pile tests. Z, depth; H, horizontal load.

Accepted manuscript doi:
10.1680/jphmg.20.00030

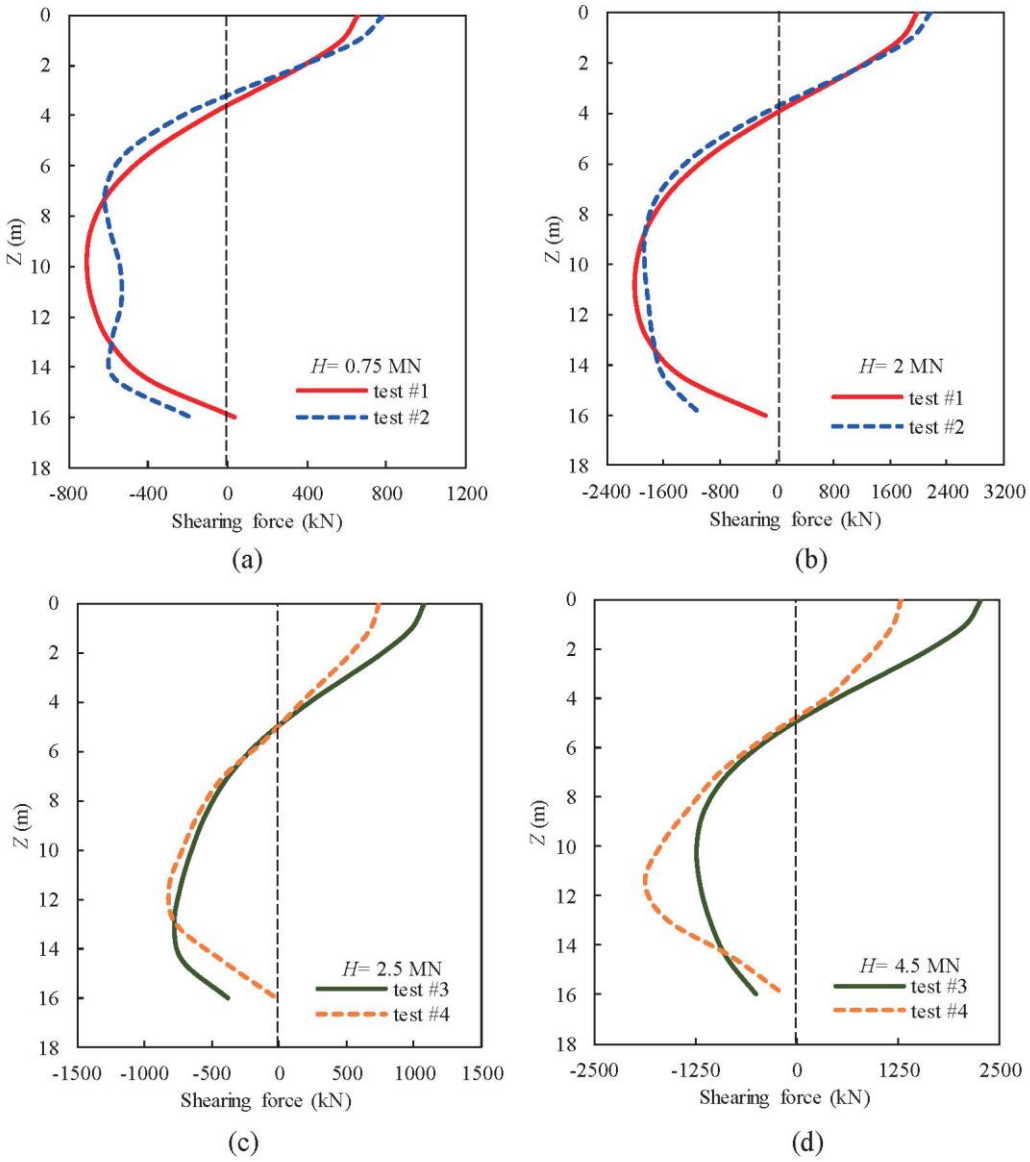

FIG. 11 Profiles of pile shearing force under different loading conditions. (a) H=0.75 MN in single-pile tests; (b) H=2 MN in single-pile tests; (c) H=2.5MN tripod-pile tests; (d) H=4.5 MN tripod-pile tests. Z, depth; H, horizontal load.

Accepted manuscript doi:
10.1680/jphmg.20.00030

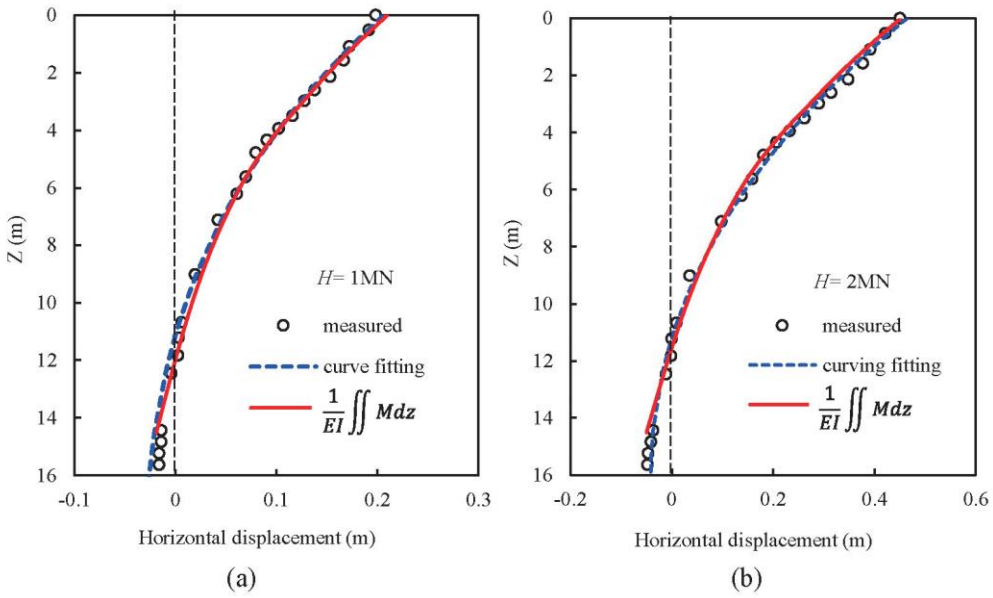

FIG. 12 Comparisons of horizontal displacement of the pile from different methods in test #1 for different horizontal forces. (a) H=0.5 MN; (b) H=1.3 MN. Z, depth; D, pile diameter; H, horizontal load.

Accepted manuscript doi:
10.1680/jphmg.20.00030

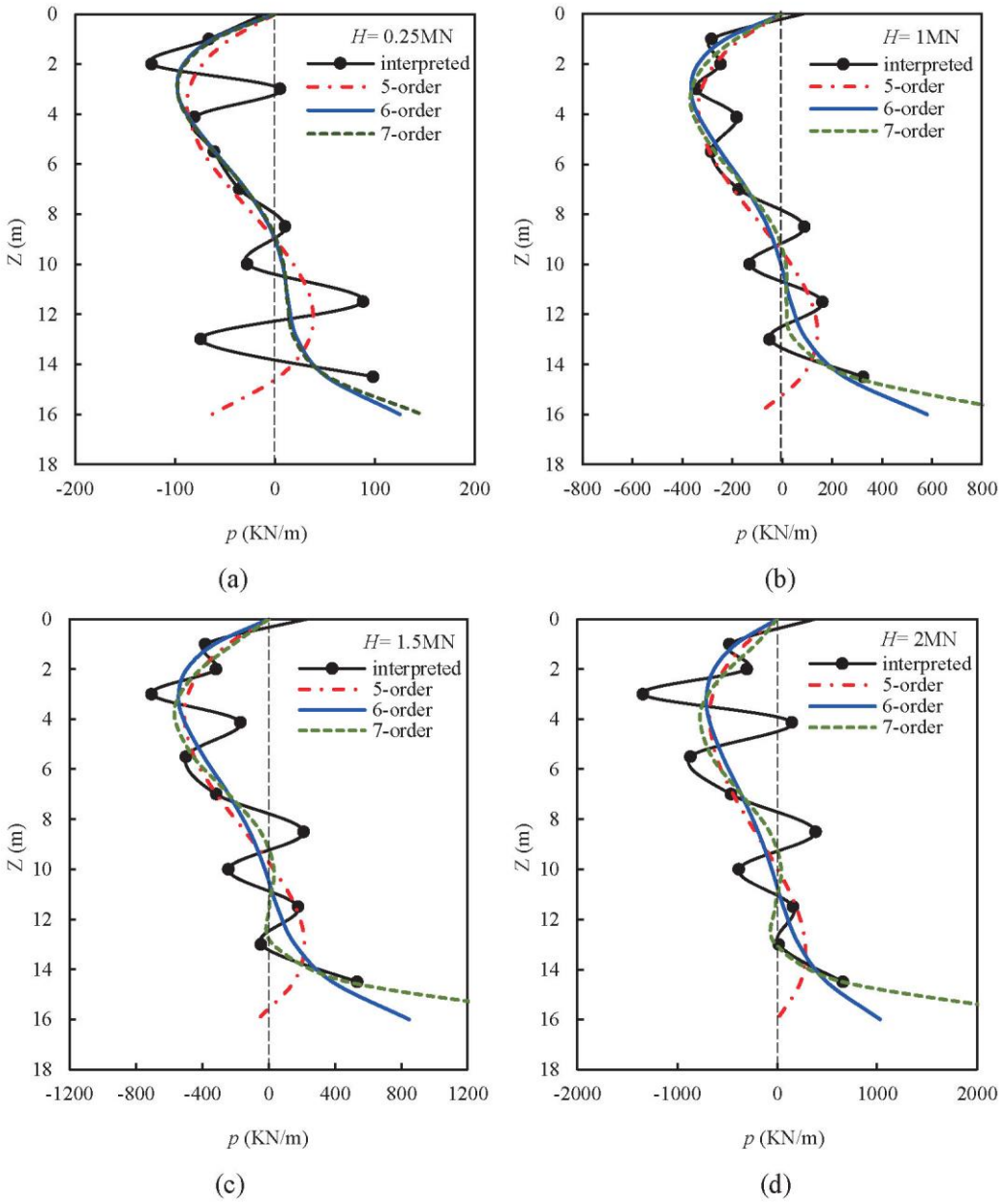

FIG. 13 Comparisons of earth pressure from different orders of polynomial curve fitting under different horizontal loads in test #1 for different horizontal forces. (a) H=0.25 MN; (b) H=1 MN; (c) H=1.5 MN; (d) H=2 MN. Z, depth; D, pile diameter; H, horizontal load; p, earth pressure.

Accepted manuscript doi:
10.1680/jphmg.20.00030

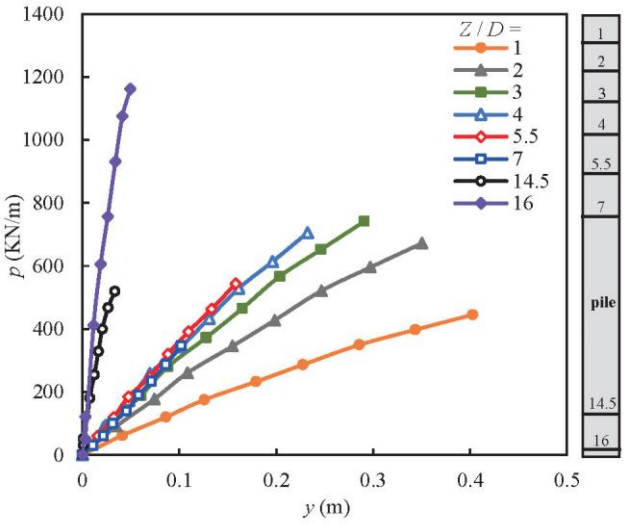

FIG. 14 *p-y* curves in pure lateral loading test at different depths. *Z*, depth; *D*, pile diameter; *p*, earth pressure; *y*, horizontal displacement.

Accepted manuscript doi:
10.1680/jphmg.20.00030

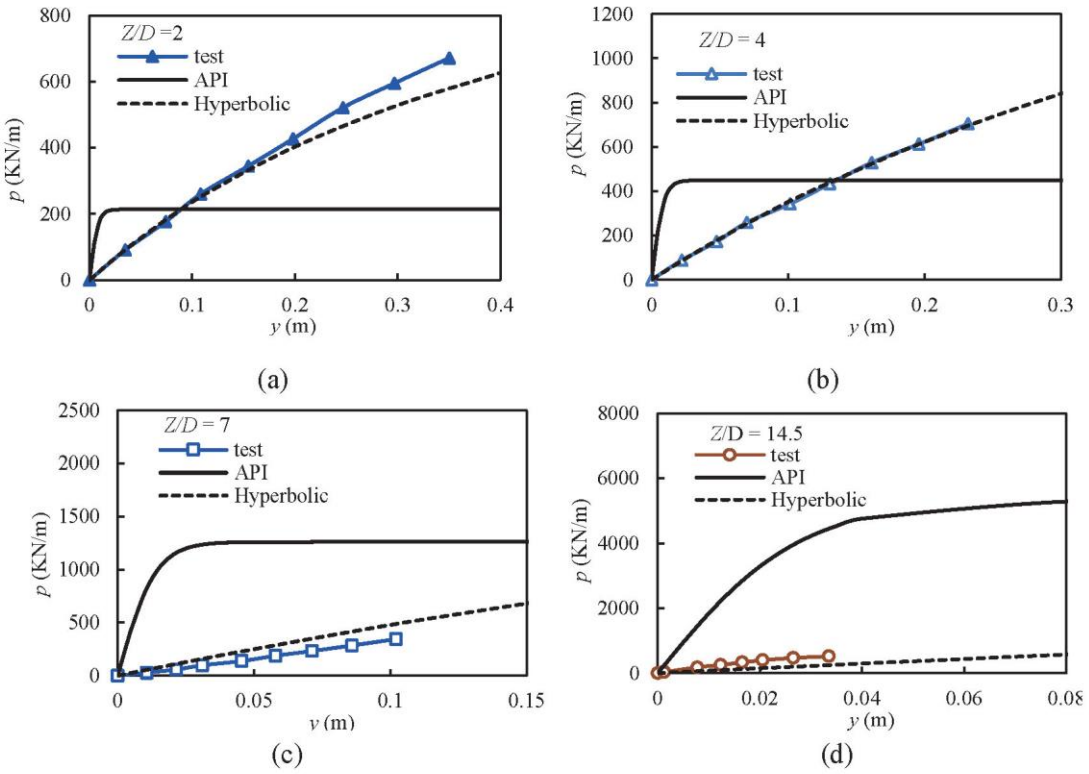

FIG. 15 Comparisons of *p*-*y* curves from pure lateral loading test with those from API for drained assumption and hyperbolic model at different depths. (a) *Z*/*D*=2; (b) *Z*/*D*=4; (c) *Z*/*D*=7; (d) *Z*/*D*=14.5. *Z*, depth; *D*, pile diameter; *p*, earth pressure; *y*, horizontal displacement.

Accepted manuscript doi:
10.1680/jphmg.20.00030

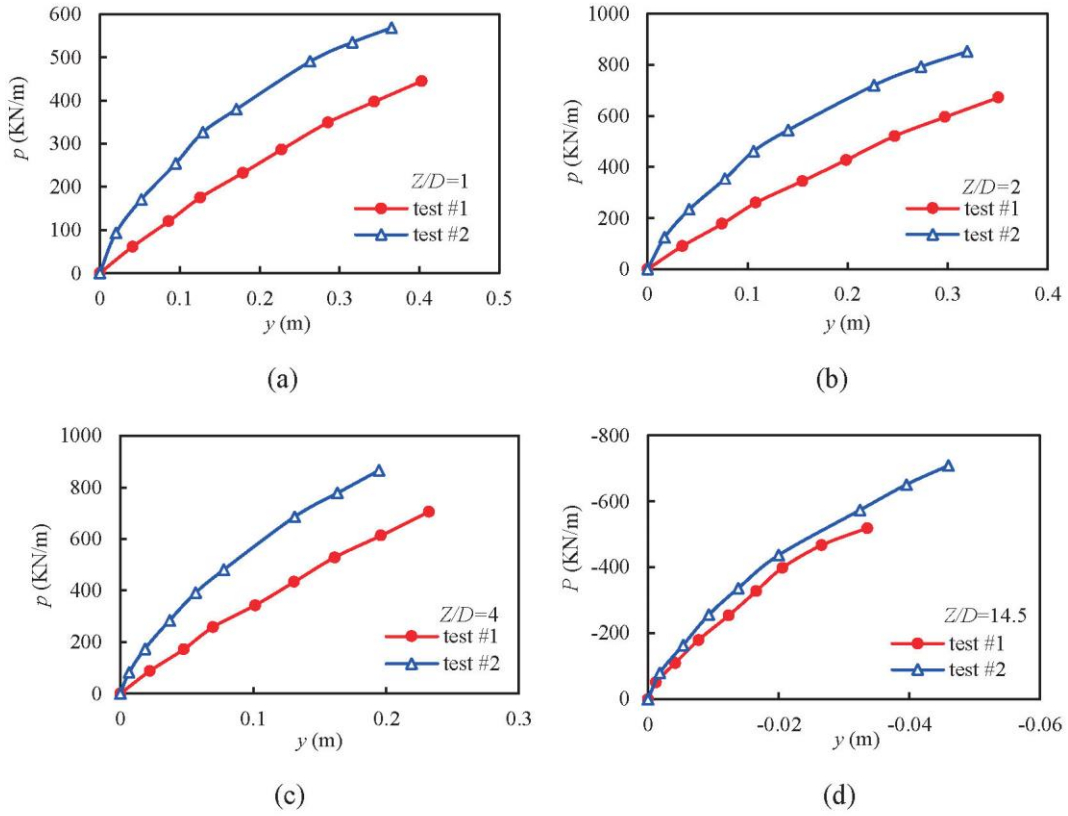

FIG. 16 Comparison of *p*-*y* curves for different loading conditions in single-pile tests at different depths. (a) *Z*/*D*=1; (b) *Z*/*D*=2; (c) *Z*/*D*=4; (d) *Z*/*D*=14.5. *Z*, depth; *D*, pile diameter; *p*, earth pressure; *y*, horizontal displacement.

Accepted manuscript doi:
10.1680/jphmg.20.00030

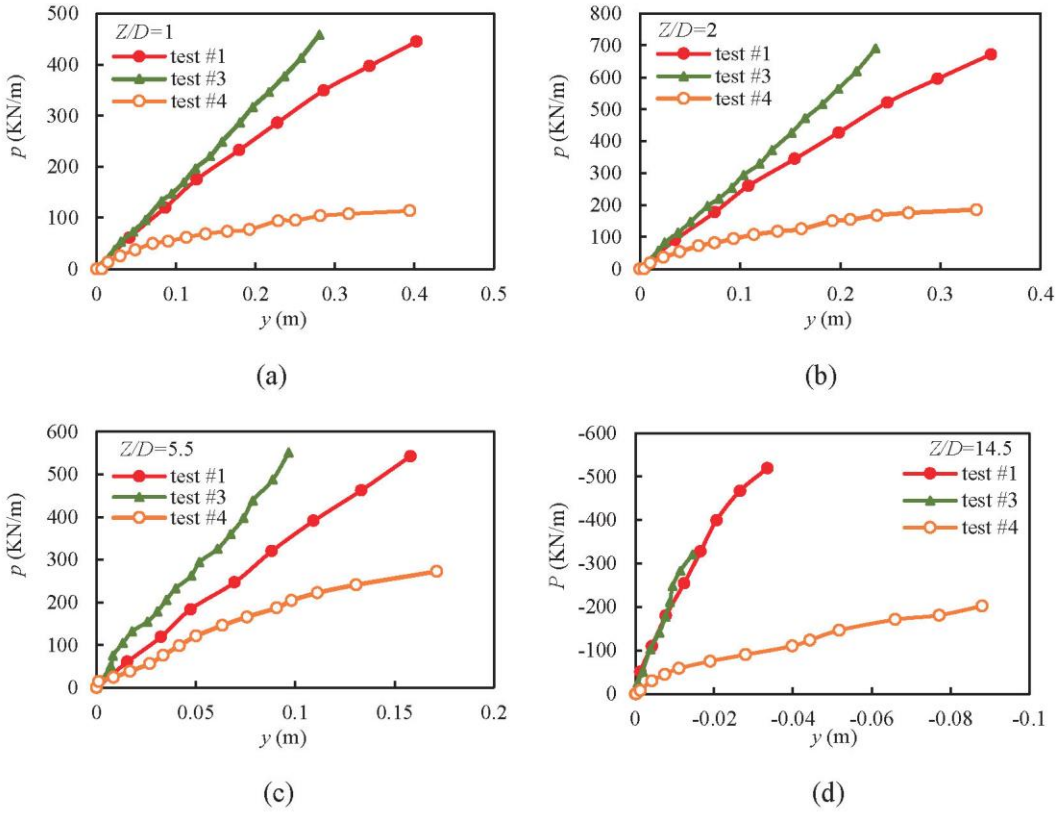

FIG. 17 Comparison of *p*-*y* curves for different loading conditions in tripod-pile tests at different depths. (a) *Z*/*D*=1; (b) *Z*/*D*=2; (c) *Z*/*D*=5.5; (d) *Z*/*D*=14.5. *Z*, depth; *D*, pile diameter; *p*, earth pressure; *y*, horizontal displacement.

Accepted manuscript doi:
10.1680/jphmg.20.00030

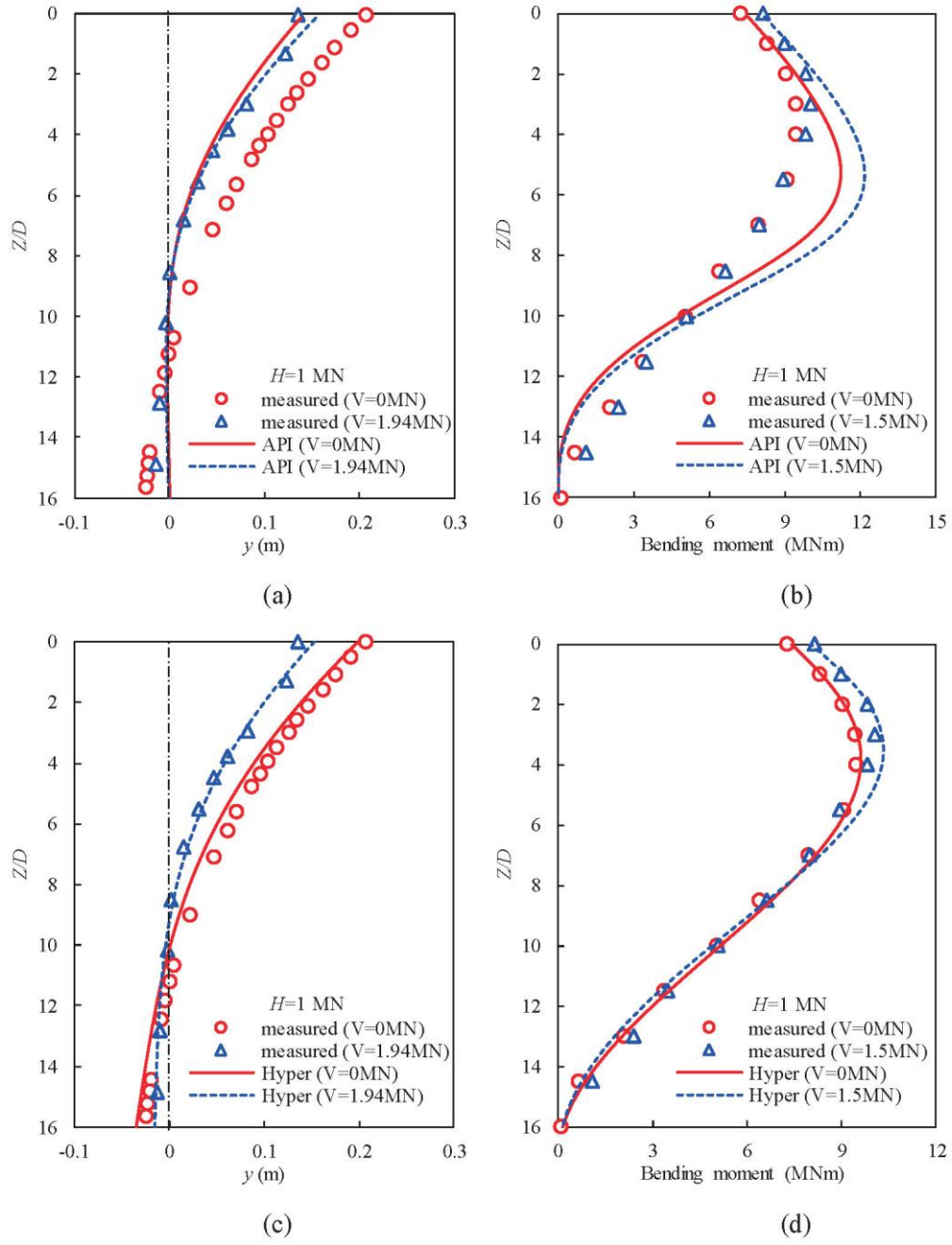

FIG. 18 Comparisons of back-calculated lateral responses of the pile from different *p-y* curves to test data. (a) lateral displacement by API *p-y* curves; (b) bending moment by API *p-y* curves; (c) lateral displacement by Hyperbolic *p-y* curves; (d) bending moment by Hyperbolic *p-y* curves. *Z*, depth; *H*, horizontal load; *V*, vertical load; *y*, horizontal displacement.

Accepted manuscript doi:
10.1680/jphmg.20.00030

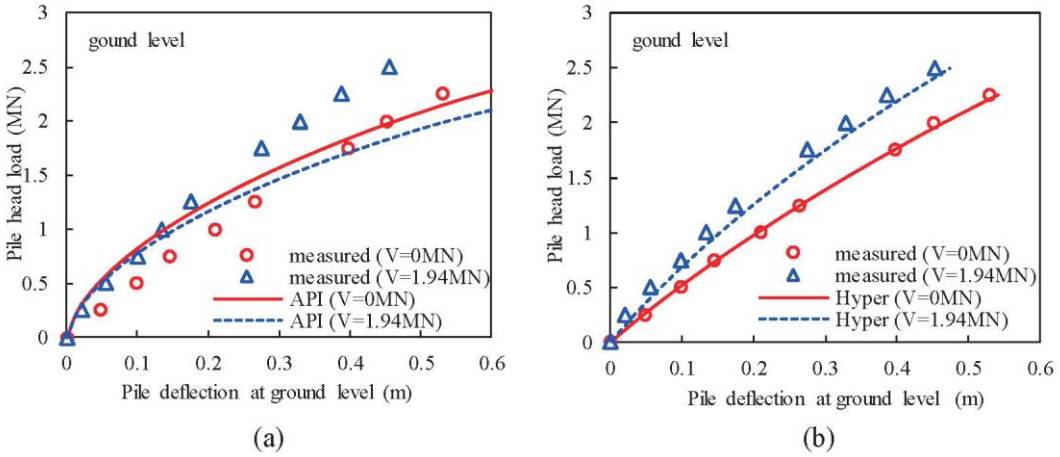

FIG. 19 Comparisons of back-calculated lateral displacement of pile at ground level from different *p-y* curves to test data. (a) from API *p-y* curve; (b) from Hyperbolic *p-y* curve. *H*, horizontal load; *V*, vertical load; *y*, horizontal displacement.